Steel and Composite Structures, *Vol. 23, No. 6 (2017) 657-668*
DOI: https://doi.org/10.12989/scs.2017.23.6.657

Using modified Halpin-Tsai approach for vibrational analysis of thick functionally graded multi-walled carbon nanotube plates

Vahid Tahouneh*

Young Researchers and Elite Club, Islamshahr Branch, Islamic Azad University, Islamshahr, Iran

(*Received October 27, 2016, Revised February 04, 2017, Accepted February 19, 2017*)

Abstract. In the most of previous studies, researchers have restricted their own studies to consider the effect of single walled carbon nanotubes as a reinforcement on the vibrational behavior of structures. In the present work, free vibration characteristics of functionally graded annular plates reinforced by multi-walled carbon nanotubes resting on Pasternak foundation are presented. The response of the elastic medium is formulated by the Winkler/Pasternak model. Modified Halpin-Tsai equation was used to evaluate the Young's modulus of the multi-walled carbon nanotube/epoxy composite samples by the incorporation of an orientation as well as an exponential shape factor in the equation. The exponential shape factor modifies the Halpin-Tsai equation from expressing a straight line to a nonlinear one in the multi-walled carbon nanotubes wt% range considered. The 2-D generalized differential quadrature method as an efficient and accurate numerical tool is used to discretize the equations of motion and to implement the various boundary conditions. The effects of two-parameter elastic foundation modulus, geometrical and material parameters together with the boundary conditions on the frequency parameters of the plates are investigated. This study serves as a benchmark for assessing the validity of numerical methods or two-dimensional theories used to analysis of annular plates.

Keywords: multi-walled carbon nanotubes; vibration; thick plates; modified Halpin-Tsai equation

1. Introduction

Nowadays, the use of carbon nanotubes in polymer/carbon nanotube composites has attracted wide attention (Wagner *et al*. 1997). A high aspect ratio, low weight of carbon nanotubes (CNTs) and their extraordinary mechanical properties (strength and flexibility) provide the ultimate reinforcement for the next generation of extremely lightweight but highly elastic and very strong advanced composite materials. On the other hand, by using of the polymer/carbon nanotube composites in advanced composite materials, we can achieve structures with low weight, high strength and high stiffness in many structures of civil, mechanical and space engineering. Several researches have recently investigated the elastic properties of multi-walled carbon nanotube (MWCNT) and their composites (Fidelus *et al*. 2005, Ghavamian *et al*. 2012). Gojny *et al*. (2005) focused on the evaluation of the different types of the carbon nanotubes applied, their influence on the mechanical properties of epoxy-based nanocomposites and the relevance of surface functionalization. Therefore, the study of the mechanical performance of carbon nanotube based composites and the discovery of possible innovative applications has recently attracted the interest of many researchers. Several researchers have reported that mechanical properties of polymeric matrices can be drastically increased (Montazeri *et al*. 2010, Yeh *et al*. 2006) by adding a few weight percent (wt%) multi-walled carbon nanotubes. Montazeri *et al*. (2010) showed that modified Halpin-Tsai equation with exponential Aspect ratio can be used to model the experimental result of MWNT composite samples. They also demonstrated that reduction in Aspect ratio (L/d) and nanotube length cause a decrease in aggregation and Above 1.5wt%, nanotubes agglomerate causing a reduction in Young's modulus values. Thus, it is important to determine the effect Aspect ratio and arrangement of carbon nanotubes on the effective properties of carbon nanotube-reinforced composite (CNTRC). Yeh *et al*. (2006) used the Halpin-Tsai equation to shows the effect of MWNT shape factor (L/d) on the mechanical properties. They showed that the mechanical properties of nanocomposite samples with the higher shape factor (L/d) values were better than the ones with the lower shape factor. The reinforcement effect of multi-walled carbon nanotubes (MWCNTs) with different aspect ratio in an epoxy matrix has been carried out by Martone *et al*. (2011). They showed that progressive reduction of the tubes effective aspect ratio occurs because of the increasing connectedness between tubes upon an increase in their concentration. Also they investigated on the effect of nanotube curvature on the average contacts number between tubes by means of the waviness that accounts for the deviation from the straight particles assumption. Marin and Marinescu (1998) studied thermoelasticity of initially stressed bodies. They first wrote the mixed initial boundary value problem within the context of thermoelasticity of initially stressed bodies. Then they

*Corresponding author, Ph.D.,
E-mail: vahid.th1982@gmail.com;
vahid.tahouneh@ut.ac.ir

ISSN: 1229-9367 (Print), 1598-6233 (Online)

established some Lagrange type identities and also introduced the Cesaro means of various parts of the total energy associated to the solutions. Marin and Lupu (1998) obtained a spatial estimate, similar to that of Saint-Venant type by using a measure of Toupin type associated with the corresponding steady-state vibration and assuming that the exciting frequency was lower to a certain critical frequency. Marin (2010) extended the concept of domain of influence in order to cover the elasticity of microstretch materials.

In structural mechanics, one of the most popular semi-analytical methods is differential quadrature method (Bellman and Casti 1971, Tahouneh 2014, 2016, Tahouneh and Naei 2015), remarkable success of which has been demonstrated by many researchers in vibration analysis of plates, shells, and beams. Liu and Liew (1999), Liew and Liu (2000) presented Differential Quadrature Method (DQM) for free vibration analysis of Mindlin isotropic circular and annular sector plates with various types of boundary conditions. A new version of the DQM was extended by Wang and Wang (2004) to analyze the free vibration of thin circular sector plates with six combinations of boundary conditions. Liew *et al*. (1996) employed differential quadrature method for free vibration analysis of moderately thick plates on Winkler foundation. Gupta *et al*. (2006) studied the free vibration analysis of non-homogeneous circular plate of non-linear thickness variation by the Differential Quadrature Method (DQM). Tornabene *et al*. (2014) studied free vibrations of free-form doubly-curved shells made of functionally graded materials using higher-order equivalent single layer theories. The partial differential system of equations was solved by using the Generalized Differential Quadrature (GDQ) method. Viola and Tornabene (2009) investigated free vibration of three and four parameter functionally graded parabolic panels and shells of revolution. For the discretization of the system equations the Generalized Differential Quadrature (GDQ) method had been used. Numerical results concerning functionally graded parabolic panels and shells showed the influence of the three parameters of the power-law distribution on their mechanical behavior. The mathematical fundamental and recent developments of differential quadrature method as well as its major applications in engineering are discussed in detail in book by Shu (2000). One can compare DQM solution procedure with the other two widely used traditional methods for plate analysis, i.e., Rayleigh-Ritz method and finite element method (FEM). The main difference between the differential quadrature method and the other methods is how the governing equations are discretized. In differential quadrature method, the governing equations and boundary conditions are directly discretized, and thus elements of stiffness and mass matrices are evaluated directly. But in Rayleigh-Ritz and finite element method (FEM), the weak form of the governing equations should be developed and the boundary conditions are satisfied in the weak form. Generally by doing so larger number of integrals with increasing amount of differentiation should be done to arrive at the element matrices. In addition, the number of degrees of freedom will be increased for an acceptable accuracy.

In comparison with research works on the free vibration or buckling analyses of FG structures (Dong 2008, Nie and Zhong 2007, 2010, Bennai *et al*. 2015, Bouchafa *et al*. 2015, Arefi 2015, Moradi-Dastjerdi 2016, Hadji *et al*. 2016, Bakora and Tounsi 2015), only a few references can be found that consider the effect of multi-walled carbon nanotube on the vibrational behavior of structures (Heshmati and Yas 2013). Farid *et al*. (2010) studied three-dimensional (3-D) temperature dependent free vibration analysis of FGM curved panels resting on two parameter elastic foundation by using a hybrid semi-analytical method. Jam *et al*. (2012) used the new version of Rule of mixture to show the effect of waviness of carbon nanotube on the vibrational behavior of nanocomposite cylindrical panel. They considered different waviness conditions with variable aspect ratio and they understood that the waviness have a significant effect on the natural frequency of nanocomposite cylindrical panel. Despite the aforementioned extensive research on the free vibration analysis of structures resting on elastic foundations, to the authors' best knowledge, still very little work has been done for vibration analysis of functionally graded-multiwalled carbon nanotube (FG-MWCNT) structures. The aim of this study is to fill this apparent gap in this area by providing the 3-D vibration analysis results for functionally graded-multiwalled carbon nanotube plates with power-law distribution of nanotube. The effective material properties of the plates are estimated using a modified Halpin-Tsai equation. Also a parametric study is carried out to highlight the influence of multi-walled carbon nanotube volume fraction in the structure thickness, type of carbon nanotube distributions and geometrical parameters on vibration behavior of functionally graded-multiwalled carbon nanotube plates.

2. Problem description

2.1 Mechanical properties of the structure

Consider an annular plate resting on two-parameter elastic foundations as shown in Fig. 1. This plate is referring to a cylindrical coordinate system (r, θ, z) as depicted in Fig. 1. It is assumed the thickness of structure is "h". The structure has continuous grading of reinforcement through thickness direction.

In this study, we will discuss about the results in the literature on mechanical properties of polymer nanotube composites. The Halpin-Tsai equation assumes that the filler are straight and uniform dispersion of the filler in the polymer matrix. The Halpin-Tsai equation (Halpin and Tsai 1969, Affdl Halpin and Kardos 1976) has been recognized for its ability to predict the modulus values for the fiber-reinforced composite samples. The effective mechanical properties of the carbon nanotube-reinforced composite (CNTRC) plate are obtained based on a modified Halpin-Tsai equation according to (Montazeri *et al*. 2010, Yeh *et al*. 2006)

$$E = E_m \frac{1+\eta_L \eta_T V_{cn}}{1-\eta_T V_{cn}}, \eta_T = \frac{\alpha E_{cn} / E_m - 1}{\alpha E_{cn} / E_m + \eta_L} \tag{1}$$

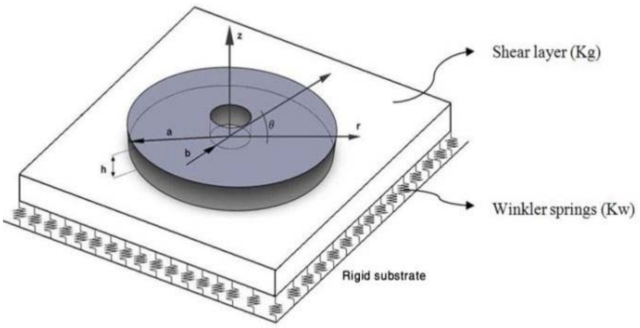

Fig. 1 Geometry of the FG-MWCNT annular plate on an elastic foundation

The effective Young's modulus of MWNT can be deduced from Eq. (1) as follows

$$E_f = \frac{(2l/d+V_{cn})\mathrm{E}-2l/d(1-V_{cn})E_m}{\alpha[(2l/\mathrm{d}+V_{cn}+1)E_m-(1-V_{cn})E]}E_m \tag{2}$$

From the linear region of the fitting line for multi-walled carbon nanotube composite/phenolic composites, the effective Young's modulus (E_f) of multi-walled carbon nanotube is 953 Gpa. In above equations, E_{cn} and E_m are the longitudinal elastic moduli of the multi-walled carbon nanotube composite and pure polymer; V_{cn} is the carbon nanotube volume fraction; η_l is the exponential shape factor; l and d are the length and the diameter of carbon nanotube and α is carbon nanotube composite orientation efficiency.

$$\eta_L = 2\frac{l}{d}e^{-aV_{cn}-b} \tag{3}$$

In which η_l is related to the aspect ratio of reinforcement length l and diameter d in the Halpin-Tsai equation. a and b are constants, related to the degree of multi-walled carbon nanotubes aggregation, which account for the nonlinear behavior of the Halpin-Tsai equation in the multi-walled carbon nanotubes wt% range considered (Montazeri *et al*. 2010, Yeh *et al*. 2006). The resulting effective properties for

Table 1 Material properties for the pure phenolic the MWCNTs

Polymer (phenolic)	MWCNTs
E_m = 5.13 Gpa	E_{cn} = 953 Gpa, ρ_{cn} = 1.03 g/ml, υ_{cn} = 0.29
ρ_m = 1.03 g/ml	a = 1/6, l = 17.57 μm, d = 23.63 nm,
υ_m = 0.34	a = 75, b = 1

the randomly oriented multi-walled carbon nanotube composite are isotropic, despite the carbon nanotubes having transversely isotropic effective properties. The orientation of a straight carbon nanotube is characterized by α. When carbon nanotubes are completely randomly oriented in the matrix, the composite is then isotropic. In this article, the experimental data for the Young's modulus of multi-walled carbon nanotubes/phenolic composites with different mass fraction of multi-walled carbon nanotubes, reported by Yeh *et al*. (2006), was used to fit the above Halpin-Tsai. In Fig. 2, the predicted Young's moduli using Eq. (1) is shown. The best fit was achieved by taking the model parameters given in Table 1. Using this prediction model, the Young's modulus of functionally graded multi-walled carbon nanotubes/phenolic composites will be estimated during the numerical solutions in the next sections. Also, the mass density and Poisson's ratio of the multi-walled carbon nanotube/phenolic composite according to rule of mixtures can be calculated, respectively, by (Shen 2009)

$$\upsilon_{ij} = V_{cn}\upsilon^{cn} + V_m\upsilon^m, \quad ij = 12,13 \ \ and \ \ 23 \qquad \rho = V_{cn}\rho^{cn} + V_m\rho^m \tag{4}$$

where υ^{cn} and ρ^{cn} are Poisson's ratio and density, respectively, of the carbon nanotube and υ^m, ρ^m are corresponding properties for the matrix.

It is assumed that the following specific power-law variation of the reinforcement volume fraction (Pelletier and Vel 2006)

$$V_{cn} = V^*_{i,cn} + (V^*_{o,cn} - V^*_{i,cn})(z/h)^p \tag{5}$$

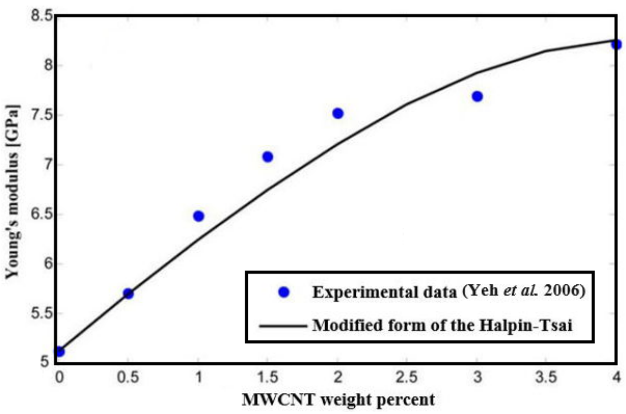

Fig. 2 Prediction of the Young's modulus of MWCNT/ phenolic composites containing various wt% of MWCNTs

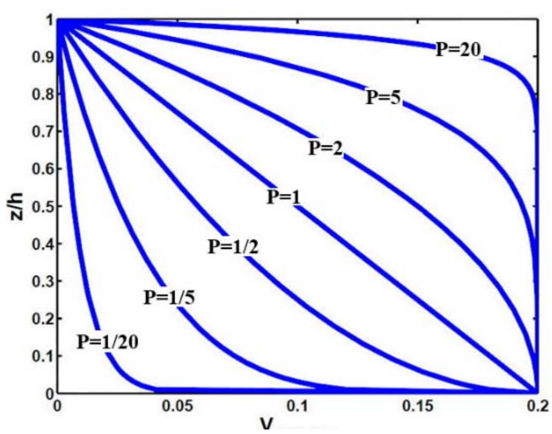

Fig. 3 Variations of the volume fraction of reinforcement (V_{MWCNT}) through the thickness of plate for different values of "*p*".

where $V^*_{i,cn}$ and $V^*_{o,cn}$ which have values that range from 0 to 0.2, denote the volume fractions of reinforcement on the lower and upper surfaces, respectively. The exponent “*P*” controls the volume fraction profile in the thickness direction of the plate. The volume fraction profile through the thickness (z/h) is illustrated in Fig. 3.

In this figure it is assumed the reinforcement volume fractions for a plate with graded fiber volume fraction are $V^*_{i,cn} = 0.2$ (20 % multi-walled carbon nanotube constituent) and $V^*_{o,cn} = 0$ (0% multi-walled carbon nanotube constituent) on the lower and upper surfaces, respectively. In this figure the reinforcement volume fraction decreases from 0.2 at $z/h = 0$ to 0 at $z/h = 1$. At z/h away from 1, the rate of increase of the reinforcement volume fraction for $p < 1$ is high compared to $p > 1$ and at z/h closer to 1, the rate of increase of the reinforcement volume fraction for $p > 1$ is much higher than for $p < 1$.

3. Governing equations

In the absence of body forces, the governing equations are as follows (Reddy 2003)

$$
\begin{aligned}
&\frac{\partial \sigma_r}{\partial r} + \frac{1}{r}\frac{\partial \tau_{r\theta}}{\partial \theta} + \frac{\partial \tau_{rz}}{\partial z} + \frac{\sigma_r - \sigma_\theta}{r} = \rho \frac{\partial^2 u_r}{\partial t^2} \\
&\frac{\partial \tau_{r\theta}}{\partial r} + \frac{1}{r}\frac{\partial \sigma_\theta}{\partial \theta} + \frac{\partial \tau_{\theta z}}{\partial z} + \frac{2\tau_{r\theta}}{r} = \rho \frac{\partial^2 u_\theta}{\partial t^2} \\
&\frac{\partial \tau_{rz}}{\partial r} + \frac{1}{r}\frac{\partial \tau_{\theta z}}{\partial \theta} + \frac{\partial \sigma_z}{\partial z} + \frac{\tau_{rz}}{r} = \rho \frac{\partial^2 u_z}{\partial t^2}
\end{aligned}
\tag{6}
$$

Where σ_r, σ_θ, σ_z are axial stress components, $\tau_{r\theta}$, $\tau_{\theta z}$, τ_{rz} are shear stress components, u_r, u_θ, u_z are displacement components, ρ denotes material density and t is time. The relations between the strain and the displacement are (Reddy 2003)

$$
\begin{aligned}
&\varepsilon_r = \frac{\partial u_r}{\partial r}, \varepsilon_\theta = \frac{u_r}{r} + \frac{1}{r}\frac{\partial u_\theta}{\partial \theta}, \varepsilon_z = \frac{\partial u_z}{\partial z}, \\
&\gamma_{\theta z} = \frac{\partial u_\theta}{\partial z} + \frac{1}{r}\frac{\partial u_z}{\partial \theta}, \gamma_{rz} = \frac{\partial u_r}{\partial z} + \frac{\partial u_z}{\partial r}, \\
&\gamma_{r\theta} = \frac{1}{r}\frac{\partial u_r}{\partial \theta} + \frac{\partial u_\theta}{\partial r} - \frac{u_\theta}{r}
\end{aligned}
\tag{7}
$$

where ε_r, ε_θ, ε_z, $\gamma_{\theta z}$, $\gamma_{r\theta}$, γ_{rz} are strain components.

The constitutive equations for orthotropic material are (Reddy 2003)

$$
\begin{Bmatrix} \sigma_r \\ \sigma_\theta \\ \sigma_z \\ \tau_{z\theta} \\ \tau_{rz} \\ \tau_{r\theta} \end{Bmatrix} =
\begin{bmatrix}
c_{11} & c_{12} & c_{13} & 0 & 0 & 0 \\
c_{12} & c_{22} & c_{23} & 0 & 0 & 0 \\
c_{13} & c_{23} & c_{33} & 0 & 0 & 0 \\
0 & 0 & 0 & c_{44} & 0 & 0 \\
0 & 0 & 0 & 0 & c_{55} & 0 \\
0 & 0 & 0 & 0 & 0 & c_{66}
\end{bmatrix}
\begin{Bmatrix} \varepsilon_r \\ \varepsilon_\theta \\ \varepsilon_z \\ \gamma_{z\theta} \\ \gamma_{rz} \\ \gamma_{r\theta} \end{Bmatrix}
\tag{8}
$$

where c_{ij} are material elastic stiffness coefficients.

Using the three-dimensional constitutive relations and the strain-displacement relations, the equations of motion in terms of displacement components for a linear elastic functionally graded (FG) plate with infinitesimal deformations can be written as

$$
\begin{aligned}
&c_{11}\frac{\partial^2 u_r}{\partial r^2} + c_{12}\left(-\frac{1}{r^2}\frac{\partial u_\theta}{\partial \theta} + \frac{1}{r}\frac{\partial^2 u_\theta}{\partial r \partial \theta} + \frac{1}{r}\frac{\partial u_r}{\partial r} - \frac{1}{r^2}u_r\right) \\
&+c_{13}\frac{\partial^2 u_z}{\partial r \partial z} + \frac{c_{66}}{r}\left(\frac{\partial^2 u_\theta}{\partial \theta \partial r} + \frac{1}{r}\frac{\partial^2 u_r}{\partial \theta^2} - \frac{1}{r}\frac{\partial u_\theta}{\partial \theta}\right) \\
&+c'_{55}\left(\frac{\partial u_r}{\partial z} + \frac{\partial u_z}{\partial r}\right) + c_{55}\left(\frac{\partial^2 u_r}{\partial z^2} + \frac{\partial^2 u_z}{\partial z \partial r}\right) + \\
&\frac{1}{r}\left[c_{11}\frac{\partial u_r}{\partial r} + c_{12}\left(\frac{1}{r}\frac{\partial u_\theta}{\partial \theta} + \frac{u_r}{r}\right) + c_{13}\frac{\partial u_z}{\partial z} - c_{12}\frac{\partial u_r}{\partial r} - c_{22}\left(\frac{1}{r}\frac{\partial u_\theta}{\partial \theta} + \frac{u_r}{r}\right) - c_{23}\frac{\partial u_z}{\partial z}\right] \\
&= \rho\frac{\partial^2 u_r}{\partial t^2}
\end{aligned}
\tag{9}
$$

$$
\begin{aligned}
&c_{66}\left(\frac{\partial^2 u_\theta}{\partial r^2} - \frac{1}{r^2}\frac{\partial u_r}{\partial \theta} + \frac{1}{r}\frac{\partial^2 u_r}{\partial r \partial \theta} + \frac{1}{r^2}u_\theta - \frac{1}{r}\frac{\partial u_\theta}{\partial r}\right) \\
&+\frac{1}{r}\left[c_{12}\frac{\partial^2 u_r}{\partial \theta \partial r} + c_{22}\left(\frac{1}{r}\frac{\partial^2 u_\theta}{\partial \theta^2} + \frac{1}{r}\frac{\partial u_r}{\partial \theta}\right) + c_{23}\frac{\partial^2 u_z}{\partial \theta \partial z}\right] \\
&+c'_{44}\left(\frac{1}{r}\frac{\partial u_z}{\partial \theta} + \frac{\partial u_\theta}{\partial z}\right) + c_{44}\left(\frac{1}{r}\frac{\partial^2 u_z}{\partial z \partial \theta} + \frac{\partial^2 u_\theta}{\partial z^2}\right) \\
&+\frac{2c_{66}}{r}\left(\frac{\partial u_\theta}{\partial r} + \frac{1}{r}\frac{\partial u_r}{\partial \theta} - \frac{u_\theta}{r}\right) = \rho\frac{\partial^2 u_\theta}{\partial t^2}
\end{aligned}
\tag{10}
$$

$$
\begin{aligned}
&c_{55}\left(\frac{\partial^2 u_r}{\partial r \partial z} + \frac{\partial^2 u_z}{\partial r^2}\right) + \frac{c_{44}}{r}\left(\frac{1}{r}\frac{\partial^2 u_z}{\partial \theta^2} + \frac{\partial^2 u_\theta}{\partial \theta \partial z}\right) \\
&+c'_{13}\frac{\partial u_r}{\partial r} + c_{13}\frac{\partial^2 u_r}{\partial z \partial r} + c'_{23}\left(\frac{1}{r}\frac{\partial u_\theta}{\partial \theta} + \frac{u_r}{r}\right) \\
&+c_{23}\left(\frac{1}{r}\frac{\partial^2 u_\theta}{\partial z \partial \theta} + \frac{1}{r}\frac{\partial u_r}{\partial z}\right) + c'_{33}\frac{\partial u_z}{\partial z} + c_{33}\frac{\partial^2 u_z}{\partial z^2} \\
&+\frac{c_{55}}{r}\left(\frac{\partial u_r}{\partial z} + \frac{\partial u_z}{\partial r}\right) = \rho\frac{\partial^2 u_z}{\partial t^2}
\end{aligned}
\tag{11}
$$

where $c'_{ij} = \dfrac{dc_{ij}}{dz}$

Eqs. (9) and (10) represent the in-plane equations of motion along the r and θ -axes, respectively; and Eq. (11) is the transverse or out-of-plane equation of motion.

The related boundary conditions are as follows:

at $z = 0$

$$
\begin{aligned}
&\tau_{zr} = 0, \tau_{z\theta} = 0 \\
&\sigma_z = K_w u_z - K_g\left(\frac{\partial^2 u_z}{\partial r^2} + \frac{1}{r}\frac{\partial u_z}{\partial r} + \frac{1}{r^2}\frac{\partial^2 u_z}{\partial \theta^2}\right)
\end{aligned}
\tag{12}
$$

at $z = h$

$$
\tau_{zr} = 0, \tau_{z\theta} = 0, \sigma_z = 0 \tag{13}
$$

K_w and K_g are the Winkler and shearing layer elastic coefficients of the foundation.

In this paper three different kinds of boundary conditions are considered: clamped-clamped (c-c), simply supported-clamped (s-c) and free-clamped (f-c). The boundary conditions at edges are

Clamped($r = b$)-Clamped($r = a$)

$$\begin{aligned} &\text{at} \quad r = a \qquad u_r = u_\theta = u_z = 0 \\ &\text{at} \quad r = b \qquad u_r = u_\theta = u_z = 0 \end{aligned} \tag{14}$$

Simply supported($r = b$)-Clamped($r = a$)

$$\begin{aligned} &\text{at} \quad r = b \qquad u_\theta = u_z = \sigma_r = 0 \\ &\text{at} \quad r = a \qquad u_r = u_\theta = u_z = 0 \end{aligned} \tag{15}$$

Free($r = b$)-Clamped($r = a$)

$$\begin{aligned} &\text{at} \quad r = a \qquad u_r = u_\theta = u_z = 0 \\ &\text{at} \quad r = b \qquad \sigma_r = \tau_{r\theta} = \tau_{rz} = 0 \end{aligned} \tag{16}$$

4. Solution procedure

Using the geometrical periodicity of the plate, the displacement components for the free vibration analysis can be represented as

$$\begin{aligned} u_r(r,\theta,z,t) &= u_{rm}(r,z)\cos(m\theta)e^{i\omega t}, \\ u_\theta(r,\theta,z,t) &= u_{\theta m}(r,z)\sin(m\theta)e^{i\omega t}, \\ u_z(r,\theta,z,t) &= u_{zm}(r,z)\cos(m\theta)e^{i\omega t} \end{aligned} \tag{17}$$

where m (= 0, 1,…, ∞) is the circumferential wavenumber; ω is the natural frequency and i $(=\sqrt{-1})$ is the imaginary number. It is obvious that $m = 0$ means axisymmetric vibration. At this stage the generalized differential quadrature method [a brief review of generalized differential quadrature method is given in Appendix A.] rules are employed to discretize the free vibration equations and the related boundary conditions. Substituting for the displacement components from Eq. (17) and then using the generalized differential quadrature rules for the spatial derivatives, the discretized form of the equations of motion at each domain grid point (r_j, z_k) with (j = 2, 3,…, $N_r - 1$) and (k = 2, 3,…, $N_z - 1$) can be obtained as

Eq. (9)

$$\begin{aligned} &(c_{11})_k \sum_{n=1}^{N_r} B^r_{jn} u_{rmnk} + (c_{12})_k \Big(\frac{-m}{r_j^2} u_{\theta mjk} \\ &+ \frac{m}{r_j} \sum_{n=1}^{N_r} A^r_{jn} u_{\theta mnk} + \frac{1}{r_j} \sum_{n=1}^{N_r} A^r_{jn} u_{rmnk} - \frac{1}{r_j^2} u_{rmjk}\Big) \\ &+ (c_{13})_k \sum_{n=1}^{N_r} \sum_{r=1}^{N_z} A^r_{jn} A^z_{kr} u_{zmnr} + \frac{(c_{66})_k}{r_j} \Big(m \sum_{n=1}^{N_r} A^r_{jn} u_{\theta mnk} \\ &- \frac{m^2}{r_j} u_{rmjk} - \frac{m}{r_j} u_{\theta mjk}\Big) + (c'_{55})_k \\ &\left(\sum_{n=1}^{N_z} A^z_{kn} u_{rmjn} + \sum_{n=1}^{N_r} A^r_{jn} u_{zmnk} \right) \\ &+ (c_{55})_k \left(\sum_{n=1}^{N_z} B^z_{kn} u_{rmjn} + \sum_{n=1}^{N_r} \sum_{r=1}^{N_z} A^r_{jn} A^z_{kr} u_{zmnr} \right) \\ &+ \frac{1}{r_j} \Big((c_{11})_k \sum_{n=1}^{N_r} A^r_{jn} u_{rmnk} + (c_{12})_k \left(\frac{m}{r_j} u_{\theta mjk} + \frac{1}{r_j} u_{rmjk} \right) \\ &+ (c_{13})_k \sum_{n=1}^{N_z} A_{kn} u_{zmjn} - (c_{12})_k \sum_{n=1}^{N_r} A^r_{jn} u_{rmnk} \\ &- (c_{22})_k \left(\frac{m}{r_j} u_{\theta mjk} + \frac{1}{r_j} u_{rmjk} \right) - (c_{23})_k \sum_{n=1}^{N_z} A^z_{kn} u_{zmjn}\Big) \\ &= -\rho_k \omega^2 u_{rmjk} \end{aligned} \tag{18}$$

Eq. (10)

$$\begin{aligned} &(c_{66})_k \Big(\sum_{n=1}^{N_r} B^r_{jn} u_{\theta mnk} + \frac{m}{r_j^2} u_{rmjk} - \frac{m}{r_j} \sum_{n=1}^{N_r} A^r_{jn} u_{rmnk} + \\ &\frac{1}{r_j^2} u_{\theta mjk} - \frac{1}{r_j} \sum_{n=1}^{N_r} A^r_{jn} u_{\theta mnk}\Big) + \frac{1}{r_j} \Big((c_{12})_k (-m) \sum_{n=1}^{N_r} A^r_{jn} u_{rmnk} \\ &+ (c_{22})_k \left(\frac{-m^2}{r_j} u_{\theta mjk} - \frac{m}{r_j} u_{rmjk} \right) - (c_{23})_k (m) \sum_{n=1}^{N_z} A^z_{kn} u_{zmjn} \\ &+ (c'_{44})_k \left(\frac{-m}{r_j} u_{zmjk} + \sum_{n=1}^{N_z} A^z_{kn} u_{\theta mjn} \right) \\ &+ (c_{44})_k \Big(\frac{-m}{r_j} \sum_{n=1}^{N_z} A^z_{kn} u_{zmjn} + \sum_{n=1}^{N_z} B^z_{kn} u_{\theta mjn}\Big) + \frac{2(c_{66})_k}{r_j} \\ &\Big(\sum_{n=1}^{N_r} A^r_{jn} u_{\theta mnk} - \frac{m}{r_j} u_{rmjk} - \frac{u_{\theta mjk}}{r_j}\Big) \\ &= -\rho_k \omega^2 u_{\theta mjk} \end{aligned} \tag{19}$$

Eq. (11)

$$\begin{aligned} &(c_{55})_k \left(\sum_{n=1}^{N_r} \sum_{r=1}^{N_z} A^z_{kr} A^r_{jn} u_{rmnr} + \sum_{n=1}^{N_r} B^r_{jn} u_{zmnk} \right) \\ &+ \frac{(c_{44})_k}{r_j} \Big(\frac{-m^2}{r_j} u_{zmjk} + (m) \sum_{n=1}^{N_z} A^z_{kn} u_{\theta mjn}\Big) \\ &+ (c'_{13})_k \sum_{n=1}^{N_z} A^z_{kn} u_{rmjn} + (c_{13})_k \sum_{n=1}^{N_r} \sum_{r=1}^{N_z} A^z_{kr} A^r_{jn} u_{rmnr} \\ &+ (c'_{23})_k \Big(\frac{m}{r_j} u_{\theta mjk} + \frac{u_{rmjk}}{r_j}\Big) + (c_{23})_k \\ &\Big(\frac{m}{r_j} \sum_{n=1}^{N_z} A^z_{kn} u_{\theta mjn} + \frac{1}{r_j} \sum_{n=1}^{N_z} A^z_{kn} u_{rmjn}\Big) + (c'_{33})_k \sum_{n=1}^{N_z} A^z_{kn} u_{zmjn} \\ &+ (c_{33})_k \sum_{n=1}^{N_z} B^z_{kn} u_{zmjn} + \frac{(c_{55})_k}{r_j} \Big(\sum_{n=1}^{N_z} A^z_{kn} u_{rmjn} \\ &+ \sum_{r=1}^{N_r} A^r_{jr} u_{zmrk}\Big) = -\rho_k \omega^2 u_{zmjk} \end{aligned} \tag{20}$$

Where A^r_{ij}, A^z_{ij} and B^r_{ij}, B^z_{ij} are the first and second order generalized differential quadrature weighting coefficients in the r- and z- directions, respectively.

In a similar manner the boundary conditions can be discretized. For this purpose, using Eq. (17) and the generalized differential quadrature discretization rules for spatial derivatives, the boundary conditions at z = 0 and h become,

Eq. (12)

at $z = 0$

$$\sum_{n=1}^{N_z} A_{kn}^z u_{rmjn} + \sum_{n=1}^{N_r} A_{jn}^r u_{zmnk} = 0,$$
$$\frac{-m}{r_j} u_{zmjk} + \sum_{n=1}^{N_z} A_{kn}^z u_{\theta mjn} = 0,$$
$$(c_{13})_k (\sum_{n=1}^{N_r} A_{jn}^r u_{rmnk}) + (c_{23})_k (\frac{m}{r_j} u_{\theta mjk} + \frac{1}{r_j} u_{rmjk}) \tag{21}$$
$$+(c_{33})_k (\sum_{n=1}^{N_z} A_{kn}^z u_{zmjn}) - K_w u_{zmjk} + K_g$$
$$(\sum_{n=1}^{N_r} B_{jn}^r u_{zmnk} + \frac{1}{r_j} \sum_{n=1}^{N_r} A_{jn}^r u_{zmnk} - \frac{m^2}{r_j^2} u_{zmjk}) = 0$$

Eq. (13)

at $z = h$

$$\sum_{n=1}^{Nz} A_{kn}^z u_{\theta mjn} + \sum_{n=1}^{Nr} A_{jn}^r u_{zmnk} = 0,$$
$$\frac{-m}{rj} u_{zmjk} + \left(\sum_{n=1}^{Nz} A_{kn}^z u_{\theta mjn} \right) = 0,$$
$$(c_{13})_k \left(\sum_{n=1}^{Nr} A_{jn}^r u_{rmnk} \right) + (c_{23})_k \left(\frac{m}{r_j} u_{\theta mjk} + \frac{1}{r_j} u_{rmjk} \right) \tag{22}$$
$$+(c_{33})_k \left(\sum_{n=1}^{Nz} A_{kn}^z u_{zmjn} \right) = 0$$

where k = 1 at z = 0 and $k = N_z$ at $z = h$, and $j = 1, 2, ..., N_r$.

The boundary conditions at $r = b$ and a stated in Eqs. (14)-(16) become,

Simply supported (S)

$$u_{zmjk} = 0, \qquad u_{\theta mjk} = 0,$$
$$(c_{11})_k (\sum_{n=1}^{N_r} A_{jn}^r u_{rmnk}) + (c_{12})_k (\frac{m}{r_j} u_{\theta mjk} + \frac{1}{r_j} u_{rmjk}) \tag{23a}$$
$$+(c_{13})_k (\sum_{n=1}^{N_z} A_{kn}^z u_{zmjn}) = 0$$

Clamped (C)

$$u_{rmjk} = 0, u_{\theta mjk} = 0, u_{zmjk} = 0 \tag{23b}$$

Free (F)

$$(c_{11})_k \sum_{n=1}^{N_r} A_{jn}^r u_{rmnk} + (c_{12})_k (\frac{m}{r_j} u_{\theta mjk} + \frac{1}{r_j} u_{rmjk}) \tag{23c}$$
$$+(c_{13})_k \sum_{n=1}^{N_z} A_{kn}^z u_{zmjn} = 0,$$
$$\frac{1}{r_j} \sum_{n=1}^{N_r} A_{jn}^r u_{\theta mnk} - \frac{m}{r_j} u_{rmjk} - \frac{1}{r_j} u_{\theta mjk} = 0, \tag{23c}$$
$$\sum_{n=1}^{N_z} A_{kn}^z u_{rmjn} + \sum_{n=1}^{N_r} A_{jn}^r u_{zmnk} = 0$$

In the above equations $k = 2, ..., N_z - 1$; also j = 1 at $r = b$ and $j = N_r$ at $r = a$.

In order to carry out the eigenvalue analysis, the domain and boundary degrees of freedom are separated and in vector forms they are denoted as $\{d\}$ and $\{b\}$, respectively. Based on this definition, the discretized form of the equilibrium equations and the related boundary conditions take the following forms

Equations of motion (18)-(20)

$$\left[[K_{db}][K_{dd}] \right] \begin{Bmatrix} \{b\} \\ \{d\} \end{Bmatrix} - \omega^2 [M] \{d\} = \{0\} \tag{24}$$

Boundary conditions (21), (22) and (23a)-(23c)

$$[K_{bd}]\{d\} + [K_{bb}]\{b\} = \{0\} \tag{25}$$

Eliminating the boundary degrees of freedom in Eq. (24) using Eq. (25), this equation become

$$\left([K] - \omega^2 [M] \{d\} \right) = \{0\} \tag{26}$$

where $[K] = [K_{dd}] - [K_{db}][K_{bb}]^{-1}[K_{bd}]$. The above eigenvalue system of equations can be solved to find the natural frequencies and mode shapes of the plates.

5. Numerical results and discussion

In order to validate the presented solution, the natural frequency of annular functionally graded plate without elastic foundation was obtained. A functionally graded annular plate with simply-supported inner radius (b = 0.1 m) and clamped outer radius (a = 1 m) was studied. It is assumed that the material properties vary exponentially $\left(c_{ij}(z) = c_{ij}^M e^{\left(\frac{\lambda z}{h}\right)}, \rho(z) = \rho^M e^{\left(\frac{\lambda z}{h}\right)} \right)$ through the thickness of the plate. Superscripts M denote the material properties of the bottom surface of the plate, λ is the material property graded index. The ratio of the thickness and the radius is 0.2. The convergence results of the first three non-dimensional natural frequencies $(\varpi = \omega h \sqrt{\rho / c_{11}})$ in which $c_{11} = \frac{E(1-\upsilon)}{(1+\upsilon)(1-2\upsilon)}$ for mentioned plate and different N_r or N_z are listed in Table 2. The same problem has been analyzed by Nie and Zhong (2007) and Dong (2008). The results are shown in Table 2 together with those from Nie and Zhong (2007) and Dong (2008), and clearly there has

Table 2 Convergence results of the first three nondimensional frequencies for FG annular plates having Simply supported ($r = b$) and Clamped ($r = a$) conditions (a = 1 m, b = 0.1 m, h/a = 0.2 m)

$N_r = N_z$	m	λ			
		1	5	10	15
7	0	0.1886	0.1331	0.0784	0.0529
9		0.1873	0.1318	0.0783	0.0536
11		0.1872	0.1316	0.0782	0.0534
13		0.1872	0.1314	0.0782	0.0535
17		0.1870	0.1315	0.0781	0.0534
(Dong 2008)		0.1871	0.1315	0.0780	0.0536
(Nie and Zhong 2007)		0.1936	-	-	-
7	1	0.1801	0.1313	0.0733	0.0475
9		0.1972	0.1394	0.0809	0.0576
11		0.1990	0.1401	0.0821	0.0579
13		0.1990	0.1401	0.0852	0.0581
17		0.1993	0.1402	0.0842	0.0582
(Dong 2008)		0.1994	0.1402	0.0840	0.0582
(Nie and Zhong 2007)		0.2050	-	-	-
7	2	0.2744	0.1955	0.1227	0.0851
9		0.2748	0.1968	0.1202	0.0842
11		0.2785	0.1973	0.1201	0.0832
13		0.2783	0.1969	0.1201	0.0831
17		0.2782	0.1967	0.1187	0.0823
(Dong 2008)		0.2781	0.1967	0.1184	0.0820
(Nie and Zhong 2007)		0.2684	-	-	-
7	3	0.3831	0.277	0.1715	0.1188
9		0.3824	0.2765	0.1697	0.1184
11		0.3824	0.2757	0.1696	0.1180
13		0.3819	0.2757	0.1692	0.1181
17		0.3819	0.2752	0.1692	0.1182
(Dong 2008)		0.3819	0.2751	0.1693	0.1182
(Nie and Zhong 2007)		-	-	-	-

Table 3 Convergence results of the first three non-dimensional frequencies for FG annular plates having Clamped ($r = b$) and Clamped($r = a$) conditions (a = 1 m, b = 0.2 m, h = 0.1 m, λ = 1), $N_r = N_z$ = 13

m	Present	(Nie and Zhong 2007)	Ansys (Nie and Zhong 2007)
0	0.0801	0.0807	0.0810
1	0.0831	0.0837	0.0839
2	0.0955	0.0961	0.0963

been good agreement between the results. The Convergence results of the first three non-dimensional frequencies ($\varpi = \omega h\sqrt{\rho / c_{11}}$) for FGM annular plates with clamped-clamped boundary condition (a = 1 m, b = 0.2 m, h = 0.1 m, λ = 1) are listed in Table 3. The same problem has been analyzed by Nie and Zhong (2007), obviously there has been good agreement between the results.

As another example, the convergence behavior and accuracy of the method for the first five frequency parameters of thick FG annular plates with both the inner and the outer surface clamped are presented in Tables 4 and 5. It is noticed there is good agreement between the present results with similar ones obtained by Dong (2008).

Table 4 Convergence study of the first five none-dimensional natural frequency parameters for free vibration of a clamped-clamped FGM annular plate

$N_r = N_z$	m	ϖ_1	ϖ_2	ϖ_3	ϖ_4	ϖ_5
7	0	8.177	13.912	15.516	19.446	20.108
9		8.201	13.875	15.511	19.481	20.158
11		8.208	13.867	15.511	19.484	20.162
13		8.210	13.870	15.511	19.485	20.164
17		8.213	13.872	15.515	19.485	20.166
(Dong 2008)		8.214	13.872	15.514	19.485	20.167
7	1	8.303	9.696	13.803	14.885	15.546
9		8.322	9.689	13.769	14.853	15.533
11		8.327	9.688	13.767	14.851	15.533
13		8.329	9.688	13.765	14.850	15.533
17		8.332	9.689	13.76	14.849	15.536
(Dong 2008)		8.333	9.689	13.766	14.850	15.535
7	2	8.849	11.160	13.842	15.638	16.561
9		8.861	11.147	13.814	15.615	16.548
11		8.863	11.146	13.812	15.615	16.549
13		8.865	11.145	13.810	15.614	16.549
17		8.868	11.145	13.811	15.614	16.550
(Dong 2008)		8.869	11.145	13.810	15.615	16.550
7	3	9.901	12.693	14.423	16.390	17.699
9		9.906	12.681	14.399	16.422	17.714
11		9.919	12.670	14.402	16.451	17.718
13		9.921	12.673	14.407	16.453	17.720
17		9.923	12.673	14.407	16.456	17.721
(Dong 2008)		9.924	12.672	14.407	16.455	17.721

$a/b = 2.5,\ h/a = 0.5,\ \lambda = 1,\ \varpi_i = \omega_{mi} h \sqrt{\frac{\rho}{(c_{44})_m}}$

In this section, we characterize the response of functionally graded multi-walled carbon nanotube plate with graded reinforcement volume fractions in the plate's thickness on an elastic foundation. The non-dimensional natural frequency, winkler and shearing layer elastic coefficients are as follows (Tahouneh and Yas 2014)

$$\Omega = \omega a^2 \sqrt{\rho_i h / D_i} \quad , \quad D_i = E_i h^3 / 12(1-\upsilon_i^2) \tag{27}$$

$$K_g = k_g\, a^2 / D_i \quad , \quad K_w = k_w\, a^4 / D_i \tag{28}$$

where ρ_i, E_i and υ_i are mechanical properties of are mechanical properties of multi-walled carbon nanotube.

The effects of variation of the Winkler elastic coefficient on the first non-dimensional natural frequency parameters of functionally graded multi-walled carbon nanotube (FG-MWCNT) annular plate and for different values of shearing layer elastic coefficient and sets of boundary conditions are

Table 4 Convergence study of the first five none-dimensional natural frequency parameters for free vibration of a clamped-clamped FGM annular plate

$N_r = N_z$	m	ϖ_1	ϖ_2	ϖ_3	ϖ_4	ϖ_5	$N_r = N_z$	m	ϖ_1	ϖ_2	ϖ_3	ϖ_4	ϖ_5
7	0	10.063	18.379	19.726	24.456	25.726	7	2	10.917	14.407	18.479	18.514	20.715
9		10.087	18.342	19.720	24.421	25.786	9		10.929	14.394	18.451	18.490	10.702
11		10.094	18.333	19.721	24.424	25.790	11		10.931	14.393	18.449	19.490	20.703
13		10.096	18.336	19.721	24.425	25.792	13		10.933	4.392	18.447	19.489	20.703
17		10.098	18.338	19.723	24.427	25.794	17		10.936	14.392	18.448	19.489	20.704
(Dong 2008)		10.099	18.338	19.724	24.426	25.794	(Dong 2008)		10.937	14.392	18.448	19.490	20.704
7	1	10.237	12.343	18.229	18.615	19.676	7	3	12.178	16.685	19.325	20.630	22.402
9		10.256	12.336	18.195	18.583	19.653	9		12.228	16.673	19.301	20.662	22.413
11		10.261	12.335	18.193	18.580	19.649	11		12.241	16.662	19.304	20.691	22.418
13		10.263	12.335	18.191	18.578	19.649	13		12.243	16.665	19.309	20.693	22.420
17		10.267	12.336	18.191	18.579	19.651	17		12.247	16.664	19.310	20.694	22.421
(Dong 2008)		10.266	12.336	18.192	18.578	19.651	(Dong 2008)		12.246	16.664	19.310	20.695	22.421

$a/b = 2.5,\ \ h/a = 0.5,\ \ \lambda = 1,\ \ \varpi_i = \omega_{mi} h \sqrt{\frac{\rho}{(c_{44})_m}}$

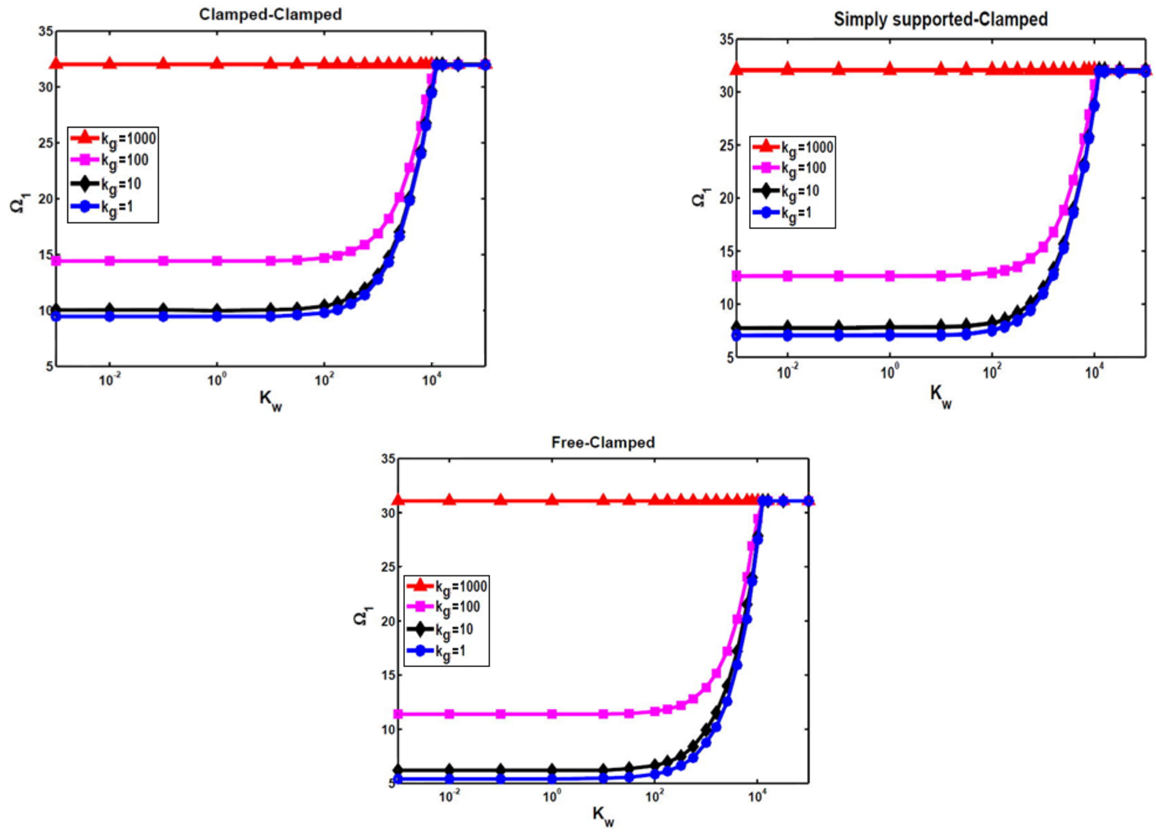

Fig. 4 Variation of the first non-dimensional natural frequency parameter of FG-MWCNT annular plate with Winkler and different shearing layer elastic coefficient for different types of boundary conditions (p = 1, h/a = 0.2, b/a = 0.2)

shown in Fig. 4. It is clear that in all cases, with increasing the elastic coefficients of the foundation, the frequency parameters increase to some limit values. In range of 10^3 to 10^4 for Winkler elastic coefficient the frequency parameter is sharply increasing, because in this range the stiffness of the plate is suddenly added to the elastic coefficient of the foundation and it results in increasing the total stiffness of the structure (= plate and foundation).

It is observed for the large values of Winkler elastic coefficient, the shearing layer elastic coefficient has less effect and the results become independent of it.

The influence of shearing layer elastic coefficient on the first non-dimensional natural frequencies for different sets of boundary conditions is shown in Fig. 5. One can see that

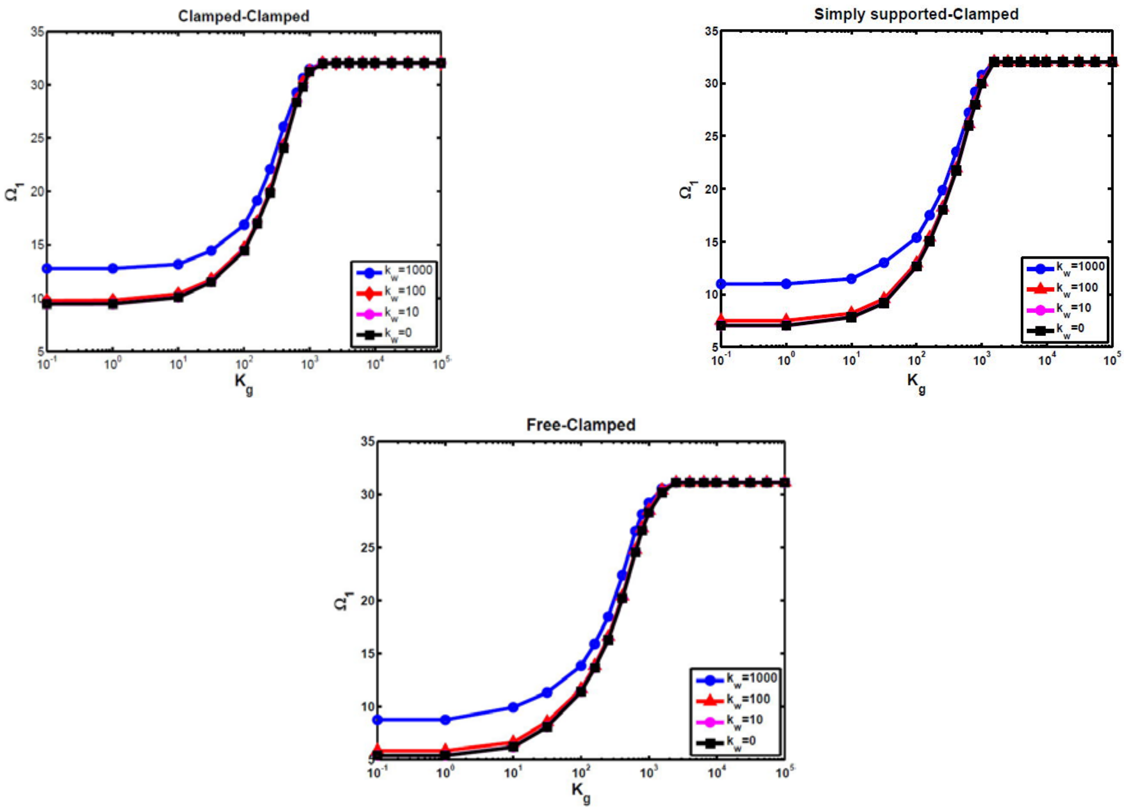

Fig. 5 Variation of the first non-dimensional natural frequency parameters of FG-MWCNT annular plates versus the shearing layer elastic coefficient for different Winkler elastic coefficient and different types of boundary conditions (p = 1, h/a = 0.2, b/a = 0.2)

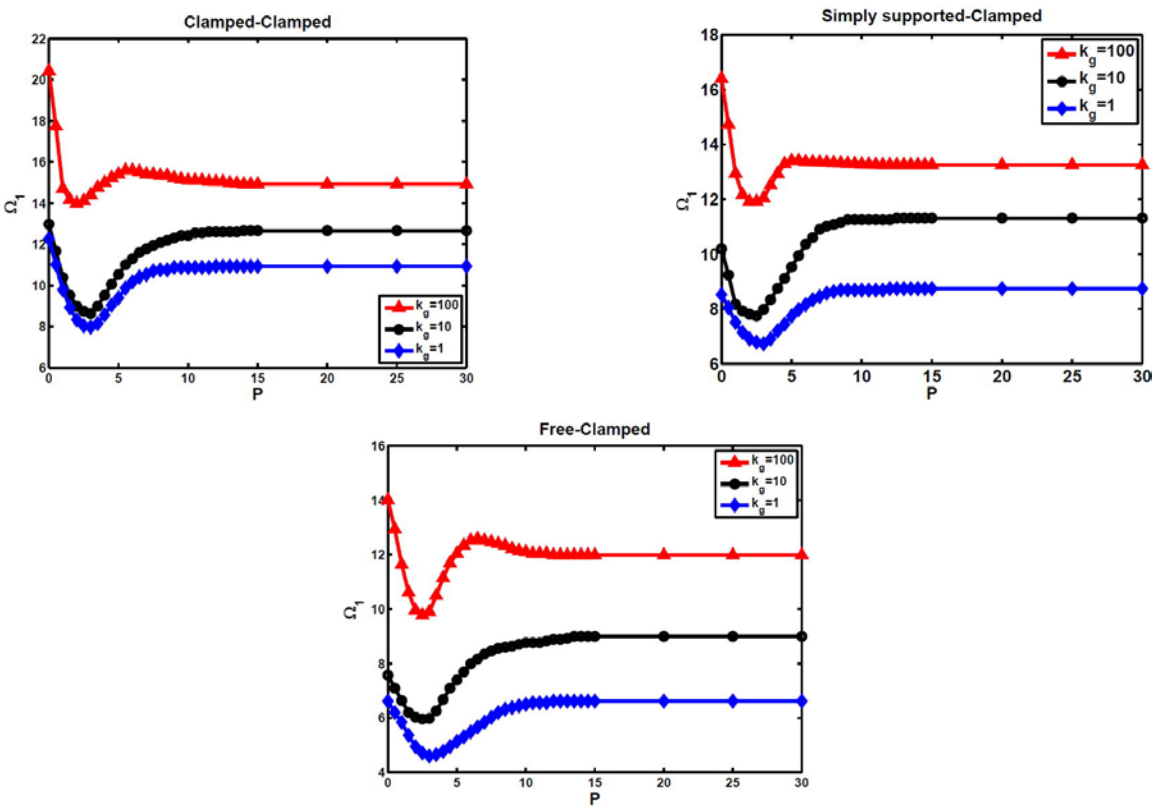

Fig. 6 Variation of the first non-dimensional natural frequency parameters of FG-MWCNT annular plates on an elastic foundation versus "p" for different shearing layer elastic coefficient and boundary conditions (K_w = 100, h/a = 0.2, b/a = 0.2)

the Winkler elastic coefficient has little effect on the non-dimensional natural frequencies at different values of shearing layer elastic coefficient.

Now the influence of reinforcement volume fraction “*p*” in the thickness direction is studied. This is carried out by varying the power-law exponent “*p*”.

Fig. 6 shows the influence of the constituent volume fraction “*p*” on the first non-dimensional natural frequencies of the multi-walled carbon nanotube plates on an elastic foundation. It is observed with increasing power-law exponent “*p*”, the first non-dimensional natural frequencies decrease sharply for small value of “*p*” ($p < 1$) and then for $p > 15$ it reaches a constant value for different values of the shearing layer elastic coefficient. It should be noted that second derivative of the curves in Fig. 3 is positive for $p < 1$ and negative for $p > 1$.

It is obvious for $p = 1$, the second derivative is equal to zero. Therefore, in Fig. 6, the curves have a first decreasing branch, followed by an increasing part, and finally they become constant for $p > 15$, because the volume fraction of the matrix gets approximately constant along the thickness of the plate.

6. Conclusions

In this research work, free vibration of continuous grading multi-walled carbon nanotube (MWCNT) annular plates on a two-parameter elastic foundation is investigated based on three-dimensional theory of elasticity. The elastic foundation is considered as a Pasternak model with adding a shear layer to the Winkler model.

Three complicated equations of motion for the plate under consideration are semi-analytically solved by using 2-D differential quadrature method. Using the 2-D differential quadrature method in the *r*- and *z*-directions, allows one to deal with functionally graded plates with arbitrary thickness distribution of material properties and also to implement the effects of the elastic foundations as a boundary condition on the lower surface of the plate efficiently and in an exact manner. The fast rate of convergence and accuracy of the method are investigated through the different solved examples.

The effects of different geometrical parameters such as the thickness-to-outer radius ratio, the elastic foundation parameters and boundary conditions on the performance of the natural frequency parameters of the functionally graded multi-walled carbon nanotube (FG-MWCNT) plates are investigated.

The main contribution of this work is to present useful results for continuous grading of multi-walled carbon nanotube reinforcement in the thickness direction of a plate on elastic foundations. It is shown that the variation of Winkler elastic coefficient has little effect on the non-dimensional natural frequencies at different values of shearing layer elastic coefficient. It is clear that in all cases, with increasing the shearing layer elastic coefficient of the foundation, the frequency parameters increase to some limit values. It is observed for the large values of shearing layer elastic coefficient; the results become independent of it. It is also shown that with increasing the elastic coefficients of the foundation, the frequency parameters increase to some limit values. It is observed for the large values of Winkler elastic coefficient, the shearing layer elastic coefficient has less effect and the results become independent of it.

It is observed that with increasing power-law exponent “*p*” the first non-dimensional natural frequencies decrease sharply for small value of “*p*” and then for $p > 15$, they become constant because the volume fraction of the matrix gets approximately constant along the thickness of the plate.

References

Affdl Halpin, J.C. and Kardos, J.L. (1976), “The Halpin-Tsai equations: A review”, *Polym. Eng. Sci.*, **16**(5), 344-352.

Arefi, M. (2015), “Elastic solution of a curved beam made of functionally graded materials with different cross sections’, *Steel Compos. Struct., Int. J.*, **18**(3), 659-672.

Bakora, A. and Tounsi, A. (2015), “Thermo-mechanical post-buckling behavior of thick functionally graded plates resting on elastic foundations”, *Struct. Eng. Mech., Int. J.*, **56**(1), 85-106.

Bellman, R. and Casti, J. (1971), “Differential quadrature and long term integration”, *J. Math. Anal. Appl.*, **34**(2), 235-238.

Bennai, R., Ait Atmane, H. and Tounsi, A. (2015), “A new higher-order shear and normal deformation theory for functionally graded sandwich beams”, *Steel Compos. Struct., Int. J.*, **19**(3), 521-546.

Bert, C.W. and Malik, M. (1996), “Differential quadrature method in computational mechanics: A review”, *Appl. Mech. Rev.*, **49**, 1-27.

Bouchafa, A., Bouiadjra, M.B., Houari, M.S.A. and Tounsi, A. (2015), “Thermal stresses and deflections of functionally graded sandwich plates using a new refined hyperbolic shear deformation theory”, *Steel Compos. Struct., Int. J.*, **18**(6), 1493-1515.

Dong, C.Y. (2008), “Three-dimensional free vibration analysis of functionally graded annular plates using the Chebyshev-Ritz method”, *Mater. Des.*, **29**(8), 1518-1525.

Farid, M., Zahedinejad, P. and Malekzadeh, P. (2010), “Three dimensional temperature dependent free vibration analysis of functionally graded material curved panels resting on two parameter elastic foundation using a hybrid semi-analytic, differential quadrature method”, *J. Mater. Des.*, **31**(1), 2-13.

Fidelus, J.D., Wiesel, E., Gojny, F.H., Schulte, K. and Wagner, H.D. (2005), “Thermo-mechanical properties of randomly oriented carbon/epoxy nanocomposites”, *Composites Part A*, **36**(11), 1555-1561.

Ghavamian, A., Rahmandoust, M. and Öchsner, A. (2012), “A numerical evaluation of the influence of defects on the elastic modulus of single and multi-walled carbon nanotubes”, *Comput. Mater. Sci.*, **62**, 110-116.

Gojny, F.H., Wichmann, M.H.G., Fiedler, B. and Schulte, K. (2005), “Influence of different carbon nanotubes on the mechanical properties of epoxy matrix composites-A comparative study”, *Compos. Sci. Technol.*, **65**(15), 2300-2313.

Gupta, U.S., Lal, R. and Sharma, S. (2006), “Vibration analysis of non-homogeneous circular plate of nonlinear thickness variation by differential quadrature method”, *J. Sound Vib.*, **298**(4), 892-906.

Hadji, L., Hassaine Daouadji, T., Ait Amar Meziane, M., Tlidji, Y. and Adda Bedia, E.A. (2016), “Analysis of functionally graded beam using a new first-order shear deformation theory”, *Struct. Eng. Mech., Int. J.*, **57**(2), 315-325.

Halpin, J.C. and Tsai, S.W. (1969), “Effects of environmental factors on composite materials”, *AFML-TR-67*-423.

Heshmati, M. and Yas, M.H. (2013), “Vibrations of non-uniform

functionally graded MWCNTs-polystyrene nanocomposite beams under action of moving load", *Mater. Des.*, **46**, 206-218.
Jam, J.E., Pourasghar, A. and Kamarian, S. (2012), "The effect of the aspect ratio and waviness of CNTs on the vibrational behavior of functionally graded nanocomposite cylindrical panels", *Polym. Compos.*, **33**(11), 2036-2044.
Liew, K.M. and Liu, F.L. (2000), "Differential quadrature method for vibration analysis of shear deformable annular sector plates", *J. Sound Vib.*, **230**(2), 335-356.
Liew, K.M., Han, J.B., Xiao, Z.M. and Du, H. (1996), "Differential quadrature method for Mindlin plates on Winkler foundation", *Int. J. Mech. Sci.*, **38**(4), 405-421.
Liu, F.L. and Liew, K.M. (1999), "Free vibration analysis of Mindlin sector plates numerical solutions by differential quadrature method", *Comput. Methods Appl. Mech. Eng.*, **177**(1-2), 77-92.
Marin, M. (2010), "A domain of influence theorem for microstretch elastic materials", *Nonlinear Anal. Real World Appl.*, **11**(5), 3446-3452.
Marin, M. and Lupu, M. (1998), "On harmonic vibrations in thermoelasticity of micropolar bodies", *J. Vib. Control*, **4**(5), 507-518.
Marin, M. and Marinescu, C. (1998), "Thermoelasticity of initially stressed bodies. Asymptotic equipartition of energies", *Int. J. Eng. Sci.*, **36**(1), 73-86.
Martone, A., Faiella, G., Antonucci, V., Giordano, M. and Zarrelli, M. (2011), "The effect of the aspect ratio of carbon nanotubes on their effective reinforcement modulus in an epoxy matrix", *Compos. Sci. Technol.*, **71**(8), 1117-1123.
Montazeri, A., Javadpour, J., Khavandi, A., Tcharkhtchi, A. and Mohajeri, A. (2010), "Mechanical properties of multi-walled carbon nanotube/epoxy composites", *Mater. Des.*, **31**(9), 4202-4208.
Moradi-Dastjerdi, R. (2016), "Wave propagation in functionally graded composite cylinders reinforced by aggregated carbon nanotube", *Struct. Eng. Mech., Int. J.*, **57**(3), 441-456.
Nie, G.J., and Zhong, Z. (2007), "Semi-analytical solution for three-dimensional vibration of functionally graded circular plates", *Comput. Methods Appl. Mech. Eng.*, **196**(49), 4901-4910.
Nie, G.J. and Zhong, Z. (2010), "Dynamic analysis of multi-directional functionally graded annular plates", *Appl. Math. Model.*, **34**(3), 608-616.
Pelletier Jacob, L. and Vel Senthil, S. (2006), "An exact solution for the steady state thermo elastic response of functionally graded orthotropic cylindrical shells", *Int. J. Solid Struct.*, **43**(5), 1131-1158.
Reddy, J.N. (2003), *Mechanics of Laminated Composite Plates and Shells: Theory and Analysis*, CRC Press Inc., (2nd Revised Edition).
Shen, H.S. (2009), "Nonlinear bending of functionally graded carbon nanotube-reinforced composite plates in thermal environments", *Compos. Struct.*, **91**(1), 9-19.
Shu, C. (2000), *Differential Quadrature and Its Application in Engineering*, Springer, Berlin.
Tahouneh, V. (2014), "Free vibration analysis of bidirectional functionally graded annular plates resting on elastic foundations using differential quadrature method", *Struct. Eng. Mech., Int. J.*, **52**(4), 663-686.
Tahouneh, V. (2016), "Using an equivalent continuum model for 3D dynamic analysis of nanocomposite plates", *Steel Compos. Struct., Int. J.*, **20**(3), 623-649.
Tahouneh, V. and Naei, M.H. (2015), "3D free vibration analysis of elastically supported thick nanocomposite curved panels with finite length and different boundary conditions via 2-D GDQ method", *Mech. Adv. Mater. Struct.*, **23**(10), 1216-1235.
Tahouneh, V. and Yas, M.H. (2014), "Influence of equivalent continuum model based on the Eshelby-Mori-Tanaka scheme on the vibrational response of elastically supported thick continuously graded carbon nanotube-reinforced annular plates", *Polym. Compos.*, **35**(8), 1644-1661.
Tornabene, F., Fantuzzi, N. and Bacciocchi, M. (2014), "Free vibrations of free-form doubly curved shells made of functionally graded materials using higher-order equivalent single layer theories", *Compos. Part B*, **67**, 490-509.
Viola, E. and Tornabene, F. (2009), "Free vibrations of three parameter functionally graded parabolic panels of revolution", *Mech. Res. Commun.*, **36**(5), 587-594.
Wagner, H.D., Lourie, O. and Feldman, Y. (1997), "Stress-induced fragmentation of multiwall carbon nanotubes in a polymer matrix", *Appl. Phys. Lett.*, **72**(2), 188-190.
Wang, X. and Wang, Y. (2004), "Free vibration analyses of thin sector plates by the new version of differential quadrature method", *Comput. Methods Appl. Mech. Eng.*, **193**(36), 3957-3971.
Yeh, M.K., Tai, N.H. and Liu, J.H. (2006), "Mechanical behavior of phenolic-based composites reinforced with multi-walled carbon nanotubes", *Carbon*, **44**(1), 1-9.

CC

Appendix

In Generalized Differential Quadrature Method (GDQM), the nth order partial derivative of a continuous function $f(x, z)$ with respect to x at a given point x_i can be approximated as a linear summation of weighted function values at all the discrete points in the domain of x, that is

$$\frac{\partial^n f(x_i, z)}{\partial x^n} = \sum_{k=1}^{N} c_{ik}^{n} f(x_{ik}, z) \quad (i = 1, 2, ..., N, n = 1, 2, ..., N-1) \tag{1}$$

Where N is the number of sampling points and c_{ij}^{n} is the x^i dependent weight coefficient. To determine the weighting coefficients c_{ij}^{n}, the Lagrange interpolation basic functions are used as the test functions, and explicit formulas for computing these weighting coefficients can be obtained as (Shu 2000)

$$c_{ij}^{(1)} = \frac{M^{(1)}(x_i)}{(x_i - x_j)M^{(1)}(x_j)}, i, j = 1, 2, ..., N, i \neq j \tag{2}$$

where

$$M^{(1)}(x_i) = \prod_{j=1, i \neq j}^{N} (x_i - x_j) \tag{3}$$

and for higher order derivatives, one can use the following relations iteratively

$$c_{ij}^{(n)} = n(c_{ii}^{(n-1)} c_{ij}^{1} - \frac{c_{ij}^{(n-1)}}{(x_i - x_j)}), \quad i, j = 1, 2, ..., N, \quad i \neq j, n = 2, 3, ..., N-1 \tag{4}$$

$$c_{ii}^{(n)} = -\sum_{j=1, i \neq j}^{N} c_{ij}^{(n)} \quad i = 1, 2, ..., N, \quad n = 1, 2, ..., N-1 \tag{5}$$

A simple and natural choice of the grid distribution is the uniform grid-spacing rule. However, it was found that nonuniform grid-spacing yields result with better accuracy. Hence, in this work, the Chebyshev-Gauss-Lobatto quadrature points are used

$$x_i = \frac{1}{2}(1 - \cos(\frac{i-1}{N-1}\pi)) \quad i = 1, 2, ..., N \tag{6}$$